Imaging the Phase Separation in Atomically Thin Buried $SrTiO_3$ Layers by Electron Channeling

L. Fitting Kourkoutis,[1] C. Stephen Hellberg,[2] V. Vaithyanathan,[3] Hao Li,[4] M. K. Parker,[1]
K. E. Andersen,[2] D. G. Schlom,[3] and D. A. Muller[1]

[1]*School of Applied and Engineering Physics, Cornell University, Ithaca, New York 14853, USA*
[2]*Center for Computational Materials Science, Naval Research Laboratory, Washington, D.C. 20375, USA*
[3]*Department of Materials Science and Engineering, Pennsylvania State University, University Park, Pennsylvania 16802-5055, USA*
[4]*Physical and Digital Realization Research, Motorola Inc., 2100 E. Elliot Road, Tempe, Arizona 85284, USA*

(Received 19 September 2007; published 23 January 2008; corrected 23 January 2008)

A phase-separation instability, resulting in the dewetting of thin $SrTiO_3$ films grown on Si(100) is shown by scanning transmission electron microscopy. Plan-view imaging of 1-nm thick, buried $SrTiO_3$ films was achieved by exploiting electron channeling through the substrate to focus the incident 0.2 nm beam down to a 0.04 nm diameter, revealing a nonuniform coverage by epitaxial $SrTiO_3$ islands and 2×1 Sr-covered regions. Density-functional calculations predict the ground state is a coexistence of 2×1 Sr-reconstructed Si and Sr-deficient $SrTiO_3$, in correspondence with the observed islanding.

DOI: 10.1103/PhysRevLett.100.036101 PACS numbers: 68.35.B−, 61.85.+p, 68.37.Lp, 68.55.−a

Perovskite oxides exhibit a wide range of electronic and magnetic properties with potential device applications. In particular, $SrTiO_3$ can be used as a buffer layer for the growth of perovskite oxide heterostructures on Si. This opens up possibilities for the incorporation of novel materials into existing Si-based technology. The $SrTiO_3$/Si interface has been studied extensively [1–11]; however, most experimental techniques rely on averaging, e.g., over large areas of the film or over the sample thickness. This also holds for electron microscopy which typically averages over 30–50 atoms in projection, depending on the sample thickness and the material. In this Letter, we report the first experimental and theoretical evidence of phase separation in thin $SrTiO_3$ films on Si (100). Here, we minimize the effect of averaging by imaging thin (<1 nm) $SrTiO_3$ films on Si in plan view, a result that is made possible by exploiting electron channeling in the silicon substrate to focus the incident 0.2 nm beam down to 0.04 nm [[12], Fig. (A)], in much the same way as a fiber plate acts as an array of microlenses for light. This new imaging mode allows us to observe an apparent dewetting or islanding of the $SrTiO_3$ layer. At equilibrium, two phases coexist, corresponding to two different interface structures. Density-functional theory (DFT) calculations confirm this coexistence and show different interface charge densities as a function of film thickness. This observation may be relevant for the successful growth of uniform $SrTiO_3$ films on Si, as it suggests that the growth has to be carried out away from equilibrium.

We used annular dark-field scanning transmission electron microscopy (ADF-STEM) to study the early stages of $SrTiO_3$ crystal growth on Si. The samples were prepared by molecular-beam epitaxy using two different growth sequences. Sequence I starts with the deposition of a 1/2 monolayer (ML) Sr template [6,10,13,14] on a (2×1) reconstructed clean Si (001) surface at 700 °C. After cooling to close to room temperature, 3 ML of epitaxial SrO followed by 2 ML of amorphous TiO_2 are deposited in high oxygen partial pressures and then heated up in vacuum until the TiO_2 reacts (a topotactic reaction) with the underlying SrO to form $SrTiO_3$ [10,11]. To study the effect of the Sr template, two additional samples were prepared as in sequence I, but with the Sr template either omitted or increased to 1 ML. In the second growth sequence (sequence II), 1–2 ML of Sr are initially deposited to promote the desorption of SiO_2 from Si [4]. A subsequent anneal at elevated temperatures (>700 °C) results in a 1/2 ML Sr template on a clean (2×1) reconstructed Si (001) surface, similar to the surface obtained with sequence I. The $SrTiO_3$ growth is then started by codeposition of Sr and Ti at substrate temperatures of about 200–300 °C and high oxygen partial pressures [6]. The low deposition temperature was chosen to study the behavior far from equilibrium. After the deposition of 2 epitaxial unit cells (uc) of $SrTiO_3$, the oxygen partial pressure is reduced and the substrate temperature increased to 500–700 °C to improve the crystallinity of the film. Finally, all films were capped with amorphous Si (*a*-Si).

For imaging we use high-angle ADF imaging, which is often referred to as *Z*-contrast imaging because the scattering contrast is strongly dependent on the atomic number [15,16]. In zone-oriented crystals, however, channeling of the electron probe along the atomic columns strongly affects the ADF image contrast. Theoretical studies of electron channeling in crystals have shown that the probe intensity at the exit surface of a crystal can be strongly enhanced [17–19], thus leading to increased visibility of an adatom [18] or of dopant atoms [20]. Here we use this effect to enhance the visibility of the thin, buried $SrTiO_3$ layer by selecting the thickness of the crystalline substrate to be close to the channeling maximum of ~15 nm, at which a fivefold narrowing of the probe is predicted [12]. Figure 1 shows plan-view ADF-STEM images of the nominal 2.5 uc thin, buried $SrTiO_3$ film grown using sequence I. Here, the sample was oriented so that the crystalline substrate constituted the entrance surface and

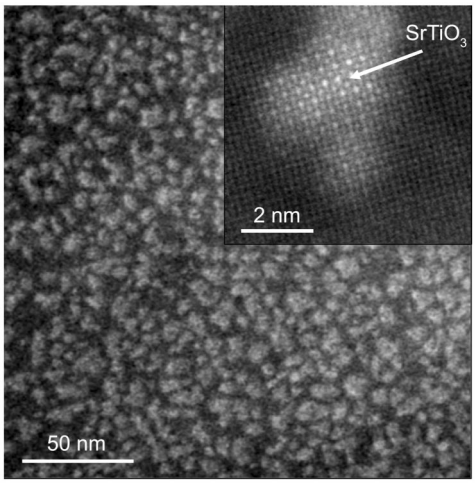

FIG. 1. Plan-view ADF-STEM image of a nominally 2.5 uc thick $SrTiO_3$ film grown on Si(100) and capped with 15 nm of *a*-Si, showing the formation of $SrTiO_3$ islands and nonuniform coverage. The $SrTiO_3$ formed at elevated temperatures in a topotactic reaction between 3 ML of epitaxial SrO and 2 ML of amorphous TiO_2, which were sequentially deposited on a $1/2$ ML Sr template on Si(100) (sequence I).

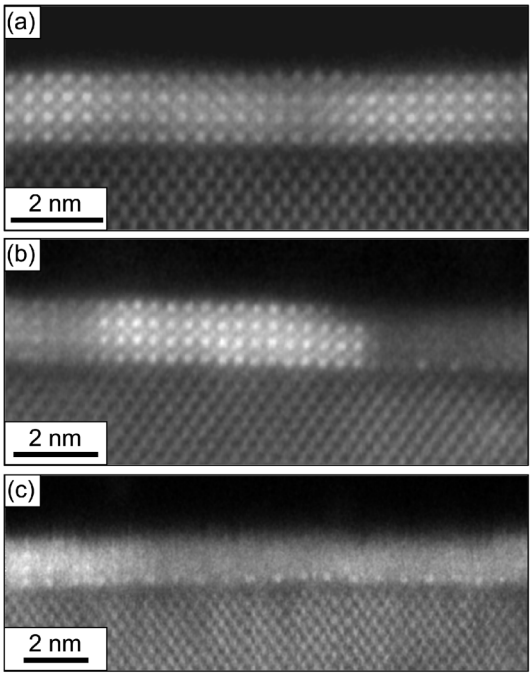

FIG. 2. Cross-sectional ADF-STEM image of a nominally 2.5 uc thick $SrTiO_3$ film grown on Si(100) and capped with 15 nm of *a*-Si. The films formed in a topotactic reaction (sequence I) on (a) a $1/2$ ML Sr template, (b) a 1 ML Sr layer, and (c) on clean Si, respectively. The average island thickness of 3.5 uc is consistent with nonuniform $SrTiO_3$ coverage. The $SrTiO_3$/Si interfaces in (b) and (c) show patches of a second stable phase: 1 ML of reconstructed Sr with double periodicity.

the thickness was chosen so that the contrast of the $SrTiO_3$ film was maximized. Surprisingly, the film is not uniform, but forms islands. The inset in Fig. 1 shows perovskite lattice spacings in the bright region [12], confirming that these patches are due to $SrTiO_3$, and suggesting that the center of an $SrTiO_3$ island is fully strained according to the lattice mismatch between Si and $SrTiO_3$. However, partial strain relaxation might occur at the edges of the islands. In the dark regions between the islands ordered $SrTiO_3$ was not detected.

Figure 2 shows cross-sectional ADF-STEM images of the nominal 2.5 uc thick $SrTiO_3$ films formed in topotactic reactions (sequence I) for various initial Sr template thicknesses. The average island height determined by cross-sectional STEM (Fig. 2) is 3.5 uc. This is consistent with nonuniform $SrTiO_3$ coverage, since the amount of $SrTiO_3$ deposited would correspond to a uniform film 2.5 uc thick. Figure 2(a) shows the $SrTiO_3$ film grown on a $1/2$ ML Sr template viewed along Si[110]. The $SrTiO_3$ appears to grow in registry on the Si substrate; however, the intensity of the $SrTiO_3$ layer varies parallel to the interface, where, in the darker regions of the film, the Ti sublattice is not resolved. These contrast variations in the cross-sectional images are expected, since for typical TEM sample thicknesses of 15–30 nm we image several islands plus the regions in between the islands in projection. Surface roughness effects due to sample preparation cannot account for the intensity variations, since the Si substrate does not show similar bright and dim regions parallel to the interface. Note that a direct determination of the interface structure of the $SrTiO_3$ islands and the Si from the cross-sectional images is not likely to be reliable, since we are probably averaging over several islands in projection. We also studied the effect of the initial Sr template on the coverage by plan-view STEM for samples with the Sr template either omitted or increased to 1 ML Sr. Plan-view STEM images of these samples [[12], Fig. (B)] reveal a significant increase in the coverage from $(12 \pm 4)\%$ to $(40 \pm 4)\%$ when the $1/2$ ML Sr template is added. A further increase of the initial Sr deposition from $1/2$ to 1 ML, however, does not lead to a further improvement of the $SrTiO_3$ coverage.

An interesting feature of the thin $SrTiO_3$ films grown on the 1 ML Sr template and without the Sr template is shown in the cross-sectional images in Figs. 2(b) and 2(c), respectively. In addition to the regions of 3.5 uc high $SrTiO_3$, there are patches that show a single layer of reconstructed Sr with double periodicity, even for the film without the Sr template layer. The cross-sectional images suggest that this layer occurs only in regions where the $SrTiO_3$ islands have not formed and hence is not covered by additional epitaxial $SrTiO_3$. Since these reconstructed Sr patches are found for samples with and without a Sr seed layer, they cannot be attributed to the Sr template, but must be inherent to the $SrTiO_3$/Si system. For the sample with a $1/2$ ML Sr template, this reconstructed layer was not observed directly, which might be explained by the relatively larger island size and hence the reduced size of the uncovered regions. Additionally, this layer of reconstructed Sr is very radia-

tion sensitive and damages quickly under the electron beam.

In order to understand the formation of islands observed in Fig. 1 and the reconstructed Sr layer, we have performed first-principles DFT calculations for $SrTiO_3$ film thicknesses from 0 to 6 ML, where the number of MLs corresponds to the number of TiO_2 layers in the structure. (0 ML is the reconstructed Sr layer to simulate the experimental Sr-templated starting surface). For each film thickness, we compute the free energy $F = E(\mathrm{DFT})\text{-}\mu_{\mathrm{Sr}}N_{\mathrm{Sr}}\text{-}\mu_{\mathrm{Ti}}N_{\mathrm{Ti}}\text{-}\mu_{\mathrm{O}}N_{\mathrm{O}}\text{-}\mu_{\mathrm{Si}}N_{\mathrm{Si}}$ for all candidate structures [1,7,21–24]. Here $E(\mathrm{DFT})$ is the DFT energy, μ_X is the chemical potential of element X, and N_X is the number of element X atoms. The calculations used the generalized-gradient approximation [25] and projector-augmented wave potentials as implemented in VASP [26]. The energies of the most stable structures are shown in Fig. 3 [27]. At 0 ML, the surface is 2×1 Sr and O reconstructed Si. At 1 ML, the favored structure has 1 ML of Sr at the interface and 0.5 ML Sr vacancies on the surface, resulting in an overall insulating system with a positively charged lower interface and negatively charged upper free surface. The surface and interface charge densities are $\pm e/a^2$ yielding a film polarization of $P = e/a^2$, where a is the in-plane cell length and e is the electron charge. When $SrTiO_3$ is lattice matched to [001] Si, the cubic pervoskite structure is distorted, and the $SrTiO_3$ can become ferroelectric [28], but the polarization in the favored 1 ML film is much larger than the equilibrium polarization of bulk $SrTiO_3$ lattice matched to Si. Figure 3 shows that as the $SrTiO_3$ becomes thicker, the structures with lower polarizations become progressively more stable. The reduced polarization requires a reduced compensating charge at the interface. In the simulation this is accomplished by reducing the interfacial Sr concentration. Experimentally, other mechanisms such as increased Si oxidation could also play a role, especially if the growth kinetics inhibited diffusion of Sr away from the interface.

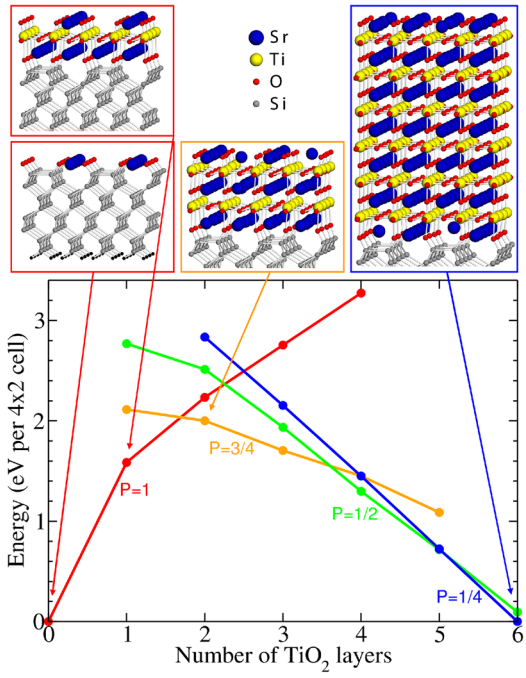

FIG. 3 (color online). Calculated total energies of $SrTiO_3$ on Si(100) as a function of film thickness. For ease of visualization, the energies have been shifted by a linear function. The Maxwell construction, which is invariant to linear shifts, shows the ground state phase separates into thick and thin regions, where the thin phase is the 2×1 Sr-reconstructed Si surface. Each structure is labeled by its electric polarization P in units of electrons per 1×1 cell. The thinner films favor a high Sr concentration in the first layer, resulting in polarization P as large as $P = 1$. As the films grow thicker, the Sr concentration in the first layer and the corresponding polarization are reduced.

According to the Maxwell construction, the energy of each structure alone (>0 ML) is higher than the energy of a mixture of two phases: one at 0 ML and the other with a thicker film. Thus, any uniform film 1 ML or thicker is unstable with respect to a phase separation into $SrTiO_3$ islands and 2×1 Sr patches. Note that the DFT energies have been shifted by a linear function so the energies at 0 ML (i.e., the 2×1 Sr surface) and 6 ML are at zero. This leaves the Maxwell construction unchanged. The 2×1 0 ML structure, shown in the top panel of Fig. 3, exhibits the same periodicity as the reconstructed Sr layer observed experimentally in Figs. 2(b) and 2(c). Ti-L and O-K electron energy loss spectroscopy of the thin films are significantly different from bulk $SrTiO_3$ suggesting the presence of defects such as vacancies in the thin film, a trend that is qualitatively captured by missing interface atoms in the lower-energy structures. Electron energy loss spectroscopy mapping to study the compositional changes across the $SrTiO_3$ film was not performed since the film was radiation sensitive, which again suggests defects in the film as bulk $SrTiO_3$ does not damage under the experimental conditions used here.

The theoretical and topotactic experimental results show that at equilibrium a thin $SrTiO_3$ film grown on Si(100) phase separates. It may be possible to obtain a more uniform film when working away from equilibrium. For that purpose we have grown thin films using sequence II, where the growth is carried out at the lowest possible temperatures for epitaxy, followed by an anneal at elevated temperatures and low oxygen partial pressure [6]. Figure 4 shows plan-view and cross-sectional ADF-STEM images of a 2 uc thin $SrTiO_3$ film grown using sequence II. The Ti sublattice in the $SrTiO_3$ film is clearly visible in the cross-sectional image [Fig. 4(b)] suggesting higher quality films. The coverage as determined from the plan-view images [Fig. 4(a)] is improved, but not complete. Hence, both growth sequences, low temperature $SrTiO_3$ epitaxy and $SrTiO_3$ formation by a topotactic reaction, result in non-uniform coverage, suggesting that this is inherent to the system.

Here we have imaged thin, buried $SrTiO_3$ layers at atomic resolution in plan-view ADF-STEM by exploiting

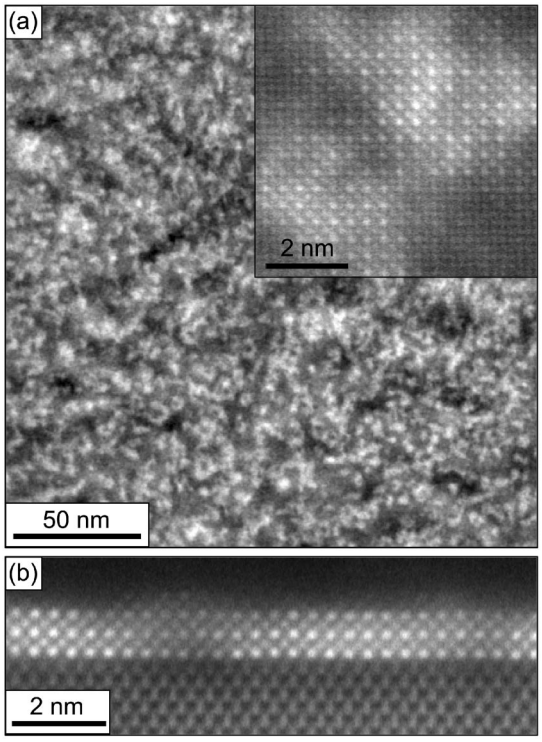

FIG. 4. (a) Plan-view and (b) cross-sectional ADF-STEM images of a nominally 2 uc thick $SrTiO_3$ film grown on Si(100) and capped with *a*-Si. The film was grown on a 1/2 ML Sr seed layer by Sr and Ti codeposition at low temperature and high oxygen partial pressure followed by an anneal at high temperature and low oxygen partial pressure (sequence II). The $SrTiO_3$ film grown under these conditions shows improved coverage, but it is still not complete.

electron channeling effects in the Si substrate. We have shown that thin $SrTiO_3$ on Si(100) will phase separate, resulting in a nonuniform coverage and the formation of $SrTiO_3$ islands, in agreement with first-principles density-functional calculations. Improved coverage was obtained by choosing growth conditions away from equilibrium.

We thank A. A. Demkov for initiating the collaboration with Motorola. The authors (L. F. K., V. V., M. K. P., D. G. S., and D. A. M.) acknowledge support under the ONR EMMA MURI monitored by Colin Wood, and by the Cornell Center for Materials Research (NSF DMR-0520404 and IMR-0417392). L. F. K. acknowledges financial support by Applied Materials. Computations were performed at the ASC DoD Major Shared Resource Center.

[1] R. A. McKee, F. J. Walker, and M. F. Chisholm, Phys. Rev. Lett. **81**, 3014 (1998).
[2] R. A. McKee, F. J. Walker, and M. F. Chisholm, Science **293**, 468 (2001).
[3] F. J. Walker and R. A. McKee, in *High Dielectric Constant Materials: VLSI MOSFET Applications*, edited by H. R. Huff and D. C. Gilmer (Springer, Berlin, 2005), pp. 607–637.
[4] W. Yi, H. Xiaoming, L. Yong, D. C. Jordan, B. Craigo, R. Droopad, Z. Yu, A. Demkov, J. L. Edwards, Jr., and W. J. Ooms, J. Vac. Sci. Technol. B **20**, 1402 (2002).
[5] H. Xiaoming, H. Li, Y. Liang, Y. Wei, Z. Yu, D. Marshall, J. Edwards, R. Droopad, X. Zhang, A. A. Demkov, K. Moore, and J. Kulik, Appl. Phys. Lett. **82**, 203 (2003).
[6] H. Li, X. Hu, Y. Wei, Z. Yu, X. Zhang, R. Droopad, A. A. Demkov, J. Edwards, K. Moore, W. Ooms, J. Kulik, and P. Fejes, J. Appl. Phys. **93**, 4521 (2003).
[7] X. Zhang, A. A. Demkov, L. Hao, X. Hu, W. Yi, and J. Kulik, Phys. Rev. B **68**, 125323 (2003).
[8] F. Amy, A. S. Wan, A. Kahn, F. J. Walker, and R. A. McKee, J. Appl. Phys. **96**, 1635 (2004).
[9] J. C. Woicik, H. Li, P. Zschack, E. Karapetrova, P. Ryan, C. R. Ashman, and C. S. Hellberg, Phys. Rev. B **73**, 024112 (2006).
[10] J. Lettieri, Ph.D. thesis, Pennsylvania State University, 2002, available online at http://etda.libraries.psu.edu/theses/approved/WorldWideIndex/ETD-202/index.html
[11] L. V. Goncharova, D. G. Starodub, E. Garfunkel, T. Gustafsson, V. Vaithyanathan, J. Lettieri, and D. G. Schlom, J. Appl. Phys. **100**, 014912 (2006).
[12] See EPAPS Document No. E-PRLTAO-100-014803 for supporting material and methods. For more information on EPAPS, see http://www.aip.org/pubservs/epaps.html.
[13] Y. Liang, S. Gan, and M. Engelhard, Appl. Phys. Lett. **79**, 3591 (2001).
[14] J. Lettieri, J. H. Haeni, and D. G. Schlom, J. Vac. Sci. Technol. A **20**, 1332 (2002).
[15] A. Howie, J. Microsc. **117**, 11 (1979).
[16] E. J. Kirkland, R. F. Loane, and J. Silcox, Ultramicroscopy **23**, 77 (1987).
[17] J. Fertig and H. Rose, Optik **59**, 407 (1981).
[18] R. F. Loane, E. J. Kirkland, and J. Silcox, Acta Crystallogr. Sect. A **44**, 912 (1988).
[19] J. M. Cowley, J. C. H. Spence, and V. V. Smirnov, Ultramicroscopy **68**, 135 (1997).
[20] P. M. Voyles, J. L. Grazul, and D. A. Muller, Ultramicroscopy **96**, 251 (2003).
[21] P. W. Peacock and J. Robertson, Appl. Phys. Lett. **83**, 5497 (2003).
[22] I. N. Yakovkin and M. Gutowski, Phys. Rev. B **70**, 165319 (2004).
[23] C. J. Forst, C. R. Ashman, K. Schwarz, and P. E. Blochl, Nature (London) **427**, 53 (2004).
[24] C. S. Hellberg *et al.* (to be published).
[25] J. P. Perdew, K. Burke, and M. Ernzerhof, Phys. Rev. Lett. **77**, 3865 (1996).
[26] G. Kresse and J. Furthmüller, Phys. Rev. B **54**, 11169 (1996); G. Kresse and D. Joubert, Phys. Rev. B **59**, 1758 (1999); P. E. Blöchl, Phys. Rev. B **50**, 17 953 (1994).
[27] The structures shown are energetically favored over the widest range of chemical potentials. In a small range of lower μ_O, structures with less O at the interface are stable. Films grown with this interface are also unstable to phase separation, in qualitative agreement with Fig. 3.
[28] J. H. Haeni, P. Irvin, W. Chang, R. Uecker, P. Reiche, Y. L. Li, S. Choudhury, W. Tian, M. E. Hawley, B. Craigo, A. K. Tagantsev, X. Q. Pan, S. K. Streiffer, L. Q. Chen, S. W. Kirchoefer, J. Levy, and D. G. Schlom, Nature (London) **430**, 758 (2004).